NASA Technical Paper 3271

December 1992

Finite-Difference Solution for Laminar or Turbulent Boundary Layer Flow Over Axisymmetric Bodies With Ideal Gas, CF_4, or Equilibrium Air Chemistry

H. Harris Hamilton II,
Daniel R. Millman,
and Robert B. Greendyke

NASA

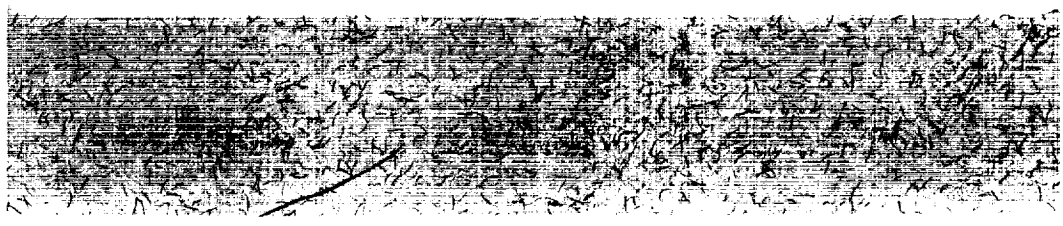

NASA Technical Paper 3271

1992

Finite-Difference Solution for Laminar or Turbulent Boundary Layer Flow Over Axisymmetric Bodies With Ideal Gas, CF_4, or Equilibrium Air Chemistry

H. Harris Hamilton II
Langley Research Center
Hampton, Virginia

Daniel R. Millman
George Washington University
Joint Institute for Advancement of Flight Sciences
Hampton, Virginia

Robert B. Greendyke
ViGYAN, Inc.
Hampton, Virginia

National Aeronautics and Space Administration
Office of Management
Scientific and Technical Information Program

Abstract

A computer code has been developed that uses an implicit finite-difference technique to solve nonsimilar, axisymmetric boundary layer equations for both laminar and turbulent flow. The code can treat ideal gases, air in chemical equilibrium, and carbon tetrafluoride (CF_4), which is a useful test gas for hypersonic blunt-body simulations. This is the only known boundary layer code that can treat CF_4. Comparisons with experimental data have demonstrated that accurate solutions are obtained. The method should prove useful as an analysis tool for comparing calculations with wind tunnel experiments and for making calculations about flight vehicles where equilibrium air chemistry assumptions are valid.

Introduction

The implicit finite-difference technique that is well established for nonsimilar, axisymmetric boundary layer equations involving laminar flow (see refs. 1 and 2) has been extended to include turbulent flow of an ideal gas (ref. 3) and reacting gas mixtures in chemical equilibrium (ref. 4). Blottner (ref. 5) has also shown that the same technique can be applied to flows where the fluid is in chemical nonequilibrium. In addition, Mayne and Adams (ref. 6) and Anderson, Moss, and Sutton (ref. 7) have used this solution technique to compute flows that include streamline swallowing. Thus, the implicit finite-difference technique provides accurate and efficient boundary layer solutions and is useful for analyzing boundary layer flows on many different types of vehicles.

A computer code is described here that uses an implicit finite-difference technique to solve nonsimilar, axisymmetric boundary layer equations for both laminar and turbulent flow. This code has been used extensively to make rapid engineering and design calculations, but it can also be used to compute the flow over a variety of three-dimensional entry vehicles through the axisymmetric analog (ref. 8). It can account for ideal gases, air in chemical equilibrium, and carbon tetrafluoride (CF_4), which is a useful test gas for hypersonic blunt-body simulations. This is the only known boundary layer code that can deal with CF_4, which is important because of the large number of CF_4 tests that require this unique capability to study the effects of variable specific heats (γ) on aerothermodynamic results.

The purpose of this paper is to document the code, give a detailed description of the method of solution, and present comparisons of calculations with data from experiments. These comparisons are presented over a wide range of body shapes, test media, and local flow conditions to demonstrate the accuracy of the approach.

Symbols

A_n	parameter defined by equation (44)
A_*	constant in equation (63)
B_n	parameter defined by equation (45)
C_n	parameter defined by equation (46)
c_p	specific heat at constant pressure, ft^2/sec^2-°R
c_v	specific heat at constant volume, ft^2/sec^2-°R
D_1	parameter defined by equation (40)
D_2	parameter defined by equation (41)
E_n	parameter defined by equation (51)
e_n	parameter defined by equation (52)
f	function defined by equation (12)
g	total enthalpy ratio, H/H_e
H	total enthalpy, ft^2/sec^2
h	static enthalpy, ft^2/sec^2
j	indicator, $j = 0$ for two-dimensional flow and $j = 1$ for axisymmetric flow
K	parameter defined by equation (42)

k	thermal conductivity, Btu/ft^2-sec-°R
k_*	constant in equation (63)
L	axial length, ft
l	parameter defined by equation (21)
l^*	parameter defined by equation (20)
l^{**}	parameter defined by equation (26)
M	Mach number
m, n	grid point across boundary layer (see fig. 2)
N_{Le}	Lewis number
N_{Pr}	frozen molecular Prandtl number
$N_{Pr,t}$	turbulent Prandtl number
N_{Re}	unit Reynolds number, ft^{-1}
p	pressure, lbf/ft^2
Q, W	general quantities defined by equation (16)
q	convective heating rate, Btu/ft^2-sec
R	gas constant, ft^2/sec^2-°R
R_n	parameter defined by equation (47)
r_N	nose radius, ft
r, z	coordinates shown in figure 1, ft
r_o	radius of axisymmetric body, ft
S	Sutherland constant (see eq. (62)), °R
T	static temperature, °R
T_r	reference temperature in Sutherland equation (62), °R
U_e	boundary layer edge velocity, ft/sec
u, v	boundary layer velocity components (see fig. 1), ft/sec
V	normal velocity defined by equation (5), ft/sec
V_∞	free-stream velocity, ft/sec
x, y	boundary layer coordinates tangent and normal to the surface (see fig. 1), ft
z	axial distance (see fig. 1), ft
α	angle of attack, deg
$\alpha_1, \alpha_2, \alpha_3, \alpha_4$	coefficients in equation (28)
β	velocity gradient parameter defined by equation (23)
γ	ratio of specific heats, c_p/c_v
$\overline{\gamma}$	intermittency factor defined by equation (66)
δ	boundary layer thickness based on velocity, ft
δ^*	boundary layer displacement thickness defined by equation (58), ft
ϵ	turbulent eddy viscosity, slug/ft-sec
θ	parameter defined by equation (22)
θ_m	boundary layer momentum thickness defined by equation (60), ft
λ	constant in equation (64)
μ	molecular viscosity, slug/ft-sec
ξ, η	transformed boundary layer coordinates defined by equations (6) and (7)
ρ	density, slugs/ft^3
τ	shear stress, lb/ft^2
ψ	stream function defined by equation (12)
ω	parameter defined by equation (27)

Subscripts:

e	boundary layer edge
inc	incompressible
s	stagnation point
w	wall
∞	free stream

Superscripts:

$\overline{(\ )}$	mean flow quantity
$(\ )'$	derivative with respect to η or fluctuating values

Method

This section presents a description of the technique used to solve the steady, compressible boundary layer equations for laminar, transitional, or turbulent flow over an axisymmetric body. The physical coordinate system used in the analysis is shown in figure 1.

Boundary Layer Equations in Physical Coordinates

The partial differential equations for a compressible, turbulent boundary layer, which express the conservation of mass, momentum, and energy, can be written as follows when the molecular and turbulent Lewis numbers are equal to 1 (see ref. 9):

$$\frac{\partial\left(\rho u r_o^j\right)}{\partial x} + \frac{\partial\left(\rho V r_o^j\right)}{\partial y} = 0 \tag{1}$$

$$\rho u \frac{\partial u}{\partial x} + \rho V \frac{\partial u}{\partial y} = -\frac{\partial p}{\partial x} + \frac{\partial}{\partial y}\left[(\mu + \epsilon)\frac{\partial u}{\partial y}\right] \tag{2}$$

$$\frac{\partial p}{\partial y} = 0 \tag{3}$$

$$\rho u \frac{\partial H}{\partial x} + \rho V \frac{\partial H}{\partial y} = \frac{\partial}{\partial y}\left\{\left[\frac{\mu}{N_{Pr}}\left(1 + \frac{\epsilon}{\mu}\frac{N_{Pr}}{N_{Pr,t}}\right)\frac{\partial H}{\partial y}\right] + \mu\left[\left(\frac{N_{Pr}-1}{N_{Pr}}\right) + \frac{\epsilon}{\mu}\left(\frac{N_{Pr,t}-1}{N_{Pr,t}}\right)\right] u \frac{\partial u}{\partial y}\right\} \tag{4}$$

where a new normal velocity has been defined as

$$V = \overline{v} + \frac{\overline{\rho' v'}}{\overline{\rho}} \tag{5}$$

The barred quantities in equation (5) represent mean flow values and the primed quantities represent fluctuating values. The j in equation (1) is equal to 0 for two-dimensional flow and to 1 for axisymmetric flow. These equations are solved subject to the boundary conditions at the wall, where $y = 0$ and

$$u = 0, \qquad V = 0, \qquad \text{and } H = H_w(x)$$

and at the outer edge, where $y \to \infty$ and

$$u \to U_e(x) \qquad \text{and } H \to H_e$$

The above boundary conditions reflect an assumption of no slip or mass injection at the wall and a prescribed wall enthalpy. The static pressure that is assumed constant across the boundary layer (see eq. (3)) is required for the boundary layer solution and, along with the edge velocity U_e, must be obtained from a separate inviscid solution. (See ref. 10.) For the types of flows considered here, the total enthalpy H_e is constant throughout the inviscid flow region.

Boundary Layer Equations in Transformed Coordinates

For help with the numerical integration of the governing equations, the physical coordinate system (x, y) can be transformed to a transformed coordinate system (ξ, η). The well-known Levy-Lees transformation (ref. 9) removes the singularity in the governing equations at $x = 0$ and reduces the growth of the boundary layer in the transformed coordinates as the solution proceeds downstream. The transformation can be written as follows:

$$\xi(x) = \int_0^x \rho_e \mu_e U_e r_o^{2j}\, dx \tag{6}$$

$$\eta(x, y) = \frac{\rho_e U_e r_o^j}{\sqrt{2\xi}} \int_0^y \frac{\rho}{\rho_e}\, dy \tag{7}$$

From equations (6) and (7) the relation between the derivatives in the physical plane (x, y) and the transformed plane (ξ, η) can be written as follows:

$$\frac{\partial}{\partial x} = \rho_e \mu_e U_e r_o^{2j} \frac{\partial}{\partial \xi} + \frac{\partial \eta}{\partial x}\frac{\partial}{\partial \eta} \tag{8}$$

$$\frac{\partial}{\partial y} = \frac{\rho U_e r_o^j}{\sqrt{2\xi}} \frac{\partial}{\partial \eta} \tag{9}$$

Now a stream function $\psi(x, y)$ can be defined that will satisfy the continuity equation (1); that is,

$$\rho u r_o^j = \frac{\partial \psi}{\partial y} \tag{10}$$

$$\rho V r_o^j = -\frac{\partial \psi}{\partial x} \tag{11}$$

If a nondimensional stream function is introduced of the form

$$\psi(\xi, \eta) = \sqrt{2\xi}\, f(\xi, \eta) \tag{12}$$

then from equations (8) (12), the following is obtained:

$$\rho u r_o^j = \rho U_e r_o^j f' \tag{13}$$

and

$$\rho V = -\rho_e \mu_e U_e r_o^j \left(\sqrt{2\xi}\frac{\partial f}{\partial \xi} + \frac{f}{\sqrt{2\xi}}\right) - \frac{1}{r_o^j}\frac{\partial \eta}{\partial x}\sqrt{2\xi}\, f' \tag{14}$$

From equation (13), the following is obtained:

$$u = U_e f' \tag{15}$$

If a general term of the form $\frac{\partial}{\partial y}(W\frac{\partial Q}{\partial y})$ is transformed using equation (9), the following can be obtained:

$$\frac{\partial}{\partial y}\left(W\,\frac{\partial Q}{\partial y}\right) = \frac{\rho U_e^2 r_o^{2j}}{2\xi}\,\frac{\partial}{\partial \eta}\left(\rho W\,\frac{\partial Q}{\partial \eta}\right) \tag{16}$$

where W and Q are general quantities. If these results are applied to equation (2), the streamwise momentum equation, the following result is obtained:

$$l^* f''' + \left(\frac{\partial l^*}{\partial \eta} + f\right) f'' - \beta\left(f'\right)^2 - \frac{2\xi}{\rho_e U_e^2}\,\frac{dp_e}{d\xi}\,\theta = 2\xi\left(f'\,\frac{\partial f'}{\partial \xi} - f''\,\frac{\partial f}{\partial \xi}\right) \tag{17}$$

From the inviscid analysis it can be shown that, if the entropy at the boundary layer edge is assumed constant,

$$\frac{dp_e}{d\xi} = -\rho_e U_e\,\frac{dU_e}{d\xi} \tag{18}$$

Based on equation (18), the transformed streamwise momentum equation (17) can be written in the form

$$l^* f''' + \left(\frac{\partial l^*}{\partial \eta} + f\right) f'' + \beta\left[\theta - \left(f'\right)^2\right] = 2\xi\left(f'\,\frac{\partial f'}{\partial \xi} - f''\,\frac{\partial f}{\partial \xi}\right) \tag{19}$$

where

$$l^* = l\left(1 + \frac{\epsilon}{\mu}\right) \tag{20}$$

$$l = \frac{\rho\mu}{\rho_e \mu_e} \tag{21}$$

$$\theta = \frac{\rho_e}{\rho} \tag{22}$$

$$\beta = \frac{2\xi}{U_e}\,\frac{dU_e}{d\xi} \tag{23}$$

When the energy equation (4) is transformed in a similar manner and the definition

$$g = \frac{H}{H_e} \tag{24}$$

is used, the following result is obtained:

$$\left(\frac{l^{**}}{N_{Pr}}\right) g'' + \left[\frac{\partial}{\partial \eta}\left(\frac{l^{**}}{N_{Pr}}\right) + f\right] g' + \omega' = 2\xi\left(f'\,\frac{\partial g}{\partial \xi} - g'\,\frac{\partial f}{\partial \xi}\right) \tag{25}$$

where

$$l^{**} = l\left(1 + \frac{\epsilon}{\mu}\,\frac{N_{Pr}}{N_{Pr,t}}\right) \tag{26}$$

$$\omega = l\left[\frac{\epsilon}{\mu}\left(1 - \frac{1}{N_{Pr,t}}\right) + \left(1 - \frac{1}{N_{Pr}}\right)\right]\left(\frac{U_e^2}{H_e} f' f''\right) \tag{27}$$

The boundary conditions for the transformed equations at the wall, where $\eta = 0$, are

$$f = 0, \qquad f' = 0, \qquad \text{and } g = g_w(\xi)$$

and at the outer edge, where $\eta \to \infty$,

$$f' \to 1 \qquad \text{and } g \to 1$$

Solution Procedure

From the approach of Blottner (ref. 11) and Davis (ref. 12), equations (19) and (25) can be written in the general form

$$\frac{\partial^2 W}{\partial \eta^2} + \alpha_1\,\frac{\partial W}{\partial \eta} + \alpha_2 W + \alpha_3 + \alpha_4\,\frac{\partial W}{\partial \xi} = 0 \tag{28}$$

where, for the momentum equation (19),

$$W = f'$$

$$\alpha_1 = \frac{\left(\frac{\partial l^*}{\partial \eta}\right) + f + 2\xi\left(\frac{\partial f}{\partial \xi}\right)}{l^*} \tag{29}$$

$$\alpha_2 = \frac{-\beta f'}{l^*} \tag{30}$$

$$\alpha_3 = \frac{\beta\theta}{l^*} \tag{31}$$

$$\alpha_4 = \frac{-2\xi f'}{l^*} \tag{32}$$

and for the energy equation (25),

$$W = g$$

$$\alpha_1 = \frac{\frac{\partial (l^{**}/N_{Pr})}{\partial \eta} + f + 2\xi\frac{\partial f}{\partial \xi}}{l^{**}/N_{Pr}} \tag{33}$$

$$\alpha_2 = 0 \tag{34}$$

$$\alpha_3 = \frac{\omega'}{l^{**}/N_{Pr}} \tag{35}$$

$$\alpha_4 = \frac{-2\xi f'}{l^{**}/N_{Pr}} \tag{36}$$

The η derivatives in equation (28) are replaced by finite-difference quotients that allow variable grid spacing in the η direction. This delineation allows grid points to be concentrated near the surface where the dependent variables change most rapidly. The ξ derivatives are replaced by two-point backward differences. A typical grid system is shown in figure 2. The solution is assumed to be known at grid point m, n and is unknown at point $m+1, n$. Adams (ref. 13) defines a nomenclature that can be applied in the following finite-difference approximations:

$$\left(\frac{\partial^2 W}{\partial \eta^2}\right)_{m+1,n} = \frac{2\left[W_{n+1} + KW_{n-1} - (1+K)W_n\right]_{m+1}}{D_2} \tag{37}$$

$$\left(\frac{\partial W}{\partial \eta}\right)_{m+1,n} = \frac{\left[W_{n+1} - K^2 W_{n-1} - \left(1-K^2\right)W_n\right]_{m+1}}{D_1} \tag{38}$$

$$\left(\frac{\partial W}{\partial \xi}\right)_{m+1,n} = \frac{W_{m+1,n} - W_{m,n}}{\Delta\xi} \tag{39}$$

where

$$D_1 = (\eta_{n+1} - \eta_n) + K^2(\eta_n - \eta_{n-1}) \tag{40}$$

$$D_2 = (\eta_{n+1} - \eta_n)^2 + K(\eta_n - \eta_{n-1})^2 \tag{41}$$

$$K = \frac{\eta_{n+1} - \eta_n}{\eta_n - \eta_{n-1}} \tag{42}$$

After substitution of equations (37) (39), the finite-difference form of equation (28) becomes

$$A_n W_{m+1,n+1} + B_n W_{m+1,n} + C_n W_{m+1,n-1} = R_n \tag{43}$$

where

$$A_n = \frac{2}{D_2} + \frac{\alpha_1}{D_1} \tag{44}$$

$$B_n = \frac{-2(1+K)}{D_2} - \frac{\alpha_1\left(1-K^2\right)}{D_1} + \alpha_2 + \frac{\alpha_4}{\Delta\xi} \tag{45}$$

$$C_n = \frac{2K}{D_2} - \frac{K^2\alpha_1}{D_1} \tag{46}$$

$$R_n = -\alpha_3 + \frac{\alpha_4 W_{3,n}}{\Delta\xi} \tag{47}$$

For the above system to be linear, the coefficients A_n, B_n, C_n, and R_n must be treated as known quantities at point m, n. Thus, equation (43) represents a set of simultaneous linear algebraic equations that must be solved for the dependent variables f' and g under the restrictions discussed above.

The system of algebraic equations represented by equation (43) is tridiagonal and may be solved efficiently by a method that Richtmyer and Morton (ref. 14) described. For a tridiagonal system, the following simple relation holds:

$$W_{m+1,n} = E_n W_{m+1,n+1} + e_n \qquad (2 \le n \le N-1) \tag{48}$$

where

$$E_2 = \frac{-A_2}{B_2} \tag{49}$$

$$e_2 = \frac{R_2 - C_2 W_{m+1,1}}{B_2} \tag{50}$$

$$E_n = \frac{-A_n}{B_n + C_n E_{n-1}} \qquad (3 \le n \le N-1) \tag{51}$$

$$e_n = \frac{R_n - C_n e_{n-1}}{B_n + C_n E_{n-1}} \qquad (3 \le n \le N-1) \tag{52}$$

For our problem, the boundary conditions at the wall ($n = 1$) and at the outer edge of the boundary layer ($n = N$) have been specified; thus, the values of $W_{m+1,1}$ and $W_{m+1,N}$ are known. The parameters E_n and e_n are evaluated by starting at $n = 2$ and moving out across the boundary layer to $n = N-1$. The solution for $W_{m+1,n}$ is then obtained by starting at $n = N-1$ and traversing back across the boundary layer to $n = 2$.

Now, because the distribution of f' across the boundary layer is known, the transformed stream function f can be determined by numerical integration of the equation

$$f(\xi,\eta) = \int_0^1 f'(\xi,\eta)\, d\eta \tag{53}$$

that uses the trapezoidal rule and the notation from the boundary conditions that $f' = 0$ at $\eta = 0$. The physical grid position across the boundary layer is obtained from the equation

$$y = \frac{\sqrt{2\xi}}{\rho_e U_e r_o^j} \int_0^\eta \frac{\rho_e}{\rho}\, d\eta \tag{54}$$

which is also integrated using the trapezoidal rule.

In this paper, the momentum and energy equations have been decoupled and linearized; thus, the solution at each station must be iterated to remove the restrictions. To linearize the equations, all quantities on the right side of equations (29) (32)

and (33) (36) are treated as known when the α coefficients are evaluated. In the first iteration at station $m+1$, these quantities are evaluated at the previous station m. In successive iterations, these coefficients are recomputed with quantities from the previous iteration. This process is repeated until the difference in the assumed and calculated quantities is less than 0.1 percent. Generally two to four iterations are required for the typical step sizes used in the present work. Numerical experiments have shown that this approach yields good results.

Boundary Layer Parameters

After the boundary layer solution has been obtained at a given body station from the procedure outlined in the previous section, several boundary layer parameters must be determined. One quantity of interest is the local convective heat flux at the wall ($y = 0$) that, for a flow with molecular and turbulent Lewis numbers equal to 1, is given by (see the appendix)

$$q_w = \left(\frac{\mu}{N_{Pr}} \frac{\partial h}{\partial y}\right)_w \tag{55}$$

where N_{Pr} is the frozen Prandtl number.

In the transformed coordinate system ξ, η, equation (55) can be written as

$$q_w = \frac{l_w \rho_e \mu_e U_e H_e r_o^j}{N_{Pr,w}\sqrt{2\xi}} g'_w \tag{56}$$

Similarly, the local shear stress at the wall is given by the equation

$$\tau_w = \mu_w \left(\frac{\partial u}{\partial y}\right)_w = \frac{l_w \rho_e \mu_e U_e^2 r_o^j}{\sqrt{2\xi}} f''_w \tag{57}$$

The derivatives appearing in equations (56) and (57) (g' and f'') are evaluated from a three-point forward difference at the wall. The displacement thickness, which is defined in physical coordinates x, y by the equation

$$\delta^* = \int_0^\infty \left(1 - \frac{\rho u}{\rho_e U_e}\right) dy \tag{58}$$

can be written in transformed coordinates ξ, η as

$$\delta^* = \frac{\sqrt{2\xi}}{\rho_e U_e r_o^j} \int_0^\infty (\theta - f')\, d\eta \tag{59}$$

Similarly, the momentum thickness, which is defined in x, y as

$$\theta_m = \int_0^\infty \frac{\rho u}{\rho_e U_e}\left(1 - \frac{u}{U_e}\right) dy \tag{60}$$

is given in ξ, η as

$$\theta_m = \frac{\sqrt{2\xi}}{\rho_e U_e r_o^j} \int_0^\infty f'(1 - f')\, d\eta \tag{61}$$

The integrals appearing in equations (59) and (61) are evaluated from the trapezoidal rule.

Transport Properties

For an ideal gas and CF_4, the molecular viscosity μ is calculated using the well-known Sutherland formula

$$\mu = \mu_r \left(\frac{T_r + S}{T + S}\right)\left(\frac{T}{T_r}\right)^{1.5} \tag{62}$$

where appropriate values are substituted for the reference temperature T_r, the reference viscosity μ_r, and the Sutherland constant S. For air in chemical equilibrium, the molecular viscosity is obtained from the data of Peng and Pindroh (ref. 15) and a table look-up procedure.

The turbulent eddy viscosity ϵ is calculated with a two-layer model. The inner region is based on a modification of Van Driest's analysis (ref. 16) introduced by Patankar and Spalding (ref. 17), and the outer region is based on the Clauser model (ref. 18) as applied by Harris (ref. 3).

The turbulent eddy viscosity for the inner region i is given by the equation

$$\left(\frac{\epsilon}{\mu}\right)_i = \frac{\rho k_*^2 y^2}{\mu}\left[1 - \exp\left(\frac{-y\sqrt{\tau\rho}}{A_*\mu}\right)\right]^2 \left|\frac{\partial u}{\partial y}\right| \tag{63}$$

where k_* and A_* are constants assumed to be approximately 0.4 and 26 in the present analysis.

The turbulent eddy viscosity for the outer region o is given by the equation

$$\left(\frac{\epsilon}{\mu}\right)_o = \frac{\rho\lambda U_e}{\mu} \delta^*_{\text{inc}} \bar{\gamma} \tag{64}$$

where λ is a constant assumed to be 0.0168, δ^*_{inc} is the incompressible displacement thickness,

$$\delta^*_{\text{inc}} = \int_0^{y_e} (1 - f')\, dy \tag{65}$$

and $\bar{\gamma}$ is Klebanoff's transverse intermittency factor (ref. 18) defined as

$$\bar{\gamma} = \frac{1 - \text{erf}\left\{5\left[(y/\delta) - 0.78\right]\right\}}{2} \tag{66}$$

which can be calculated approximately by the equation (ref. 4)

$$\bar{\gamma} \approx \frac{1}{1 + 5.5\,(y/\delta)^6} \tag{67}$$

The boundary separating the inner and outer regions is defined as the location where

$$\left(\frac{\epsilon}{\mu}\right)_i = \left(\frac{\epsilon}{\mu}\right)_o \tag{68}$$

For ideal gases and CF_4, the molecular Prandtl number is assumed constant; however, for air in chemical equilibrium, the molecular Prandtl number is obtained from the data of Peng and Pindroh (ref. 15) and a table look-up procedure. The turbulent Prandtl number is assumed constant; for all results presented in this paper, the turbulent Prandtl number is taken as 0.9.

Thermodynamic Properties

For an ideal gas, the thermodynamic properties are obtained from the ideal gas equation of state

$$p = \rho \left(\frac{R}{c_p}\right) h \tag{69}$$

based on the appropriate values for the gas constant R and the specific heat c_p. For CF_4 the thermodynamic properties are obtained from the curve fits of Sutton (ref. 19); however, for air in chemical equilibrium, the thermodynamic properties are obtained from Hansen (ref. 20) and a table look-up procedure.

Results and Discussion

In this section, results from the present method are compared with experimental data. Two gases are considered: air (either ideal gas or equilibrium chemistry options) and CF_4. Comparisons are shown for laminar and turbulent flow. For all results, the boundary layer edge conditions were obtained from the inviscid code of reference 10, except where noted otherwise.

Ideal Gas

Surface heat transfer distributions for flow over a sphere are presented in figure 3 along with experimental data measured in the Langley 31-Inch Mach 10 Tunnel (provided by John Micol of the Langley Space Systems Division). The results shown in figure 3(a) are for a Reynolds number of 2.4×10^5 per foot and those in figure 3(b) are for 5.4×10^5 per foot. In both cases the flow is laminar and the air was assumed to behave as an ideal gas with $\gamma = 1.4$. For the computed results shown in figure 3, a grid of 101 points across the boundary layer was used with the values of $\eta_{\max}$ and K set to 7.0 and 1.04, respectively. This method produced a value of $\Delta\eta$ at the wall equal to 0.005656. For both cases the computed results agree well with the experimental data (i.e., within ± 10 percent). Similar computations were performed that used 201 points across the boundary layer (results not shown) to check the adequacy of the grid, but that approach was found to have very little effect on the computed heating rates.

The next case considered is the flow over a spherically blunted 8° half-angle cone at $M = 5$ and $\alpha = 0°$. The results for this case are presented in figures 4(a) and 4(b) for $N_{Re} = 2.09 \times 10^6$ and 19.8×10^6 per foot, respectively. The experimental data for this case are from reference 21. For the lower Reynolds number (fig. 4(a)), the flow is completely laminar, and, except for just downstream of the stagnation point, the present calculations are in excellent agreement with the data. At the higher Reynolds number (fig. 4(b)), transition starts on the nose of the body near $x/r_N \approx 0.3$, and the flow is fully turbulent near $x/r_N \approx 0.8$. This case was modeled in the present calculations based on a finite transition region starting at $x/r_N = 0.3$ that followed the approach of reference 22. The results generally agree well with the experimental data.

The next comparison, presented in figure 5, is for flow over a spherically blunted, 70° half-angle cone at $M_\infty = 9.86$, $N_{Re} = 0.55 \times 10^6$ per foot, and $\alpha = 0°$. The experimental data were obtained in the Langley 31-Inch Mach 10 Tunnel by Charles Miller and Ray Midden, also of the Langley Space Systems Division. The data are the same as those used in reference 23. This configuration had a sharp corner at the trailing edge. Because of the free-stream conditions and the large half-angle cone, the entire shock layer is subsonic, with the sonic line attaching near the corner in a strong expansion region. The flow field was computed over this body based on the time-dependent method of reference 10 and a geometry comprising a spherically blunted 70° half-angle cone forebody with a trailing 40° cone frustum that caused the sonic line to attach at the corner. As the flow moves away from the stagnation point, it expands and the heating decreases as would be expected. However, as the flow approaches the trailing edge, the heating increases rapidly, reaching a peak only slightly below the stagnation value. This rapid rise in heating near the trailing edge is the result of the strong expansion in this region (i.e., large increase in the velocity gradient). Some scatter is evident in the experimental data around the stagnation

point, but the calculations generally yield very good agreement with the data over the remainder of the body.

The next case considered is the turbulent flow of ideal gas over a flat plate. For this case the calculated turbulent velocity profiles are compared with experimental data from reference 24 in figures 6(a) 6(c) for Mach numbers of 1.982, 3.701, and 4.554, respectively. The air was assumed to be an ideal gas with $\gamma = 1.4$. For the computed results shown in figure 6, a grid of 201 points across the boundary layer was used with the values of $\eta_{\max}$ and K set to 100 and 1.09, respectively. This setting produced a value of $\Delta\eta$ at the wall equal to 0.2944×10^{-6}. The increase in the number of grid points was required to resolve the large gradients in the turbulent flow velocity profile near the surface. For each Mach number, the calculated results are in excellent agreement with the experimental data (i.e., within ± 5 percent).

Through numerical experimentation, a grid of 101 points with $\eta_{\max} = 7.0$ and $K = 1.04$ has been found to provide good heat transfer results for most laminar flow cases; for most turbulent flows, a grid of 101 to 201 points with $\eta_{\max} = 100$ and $K = 1.09$ appears to provide good heat transfer results. Thus, these grids appear to be adequate for most problems.

The computed results obtained thus far for perfect gases and laminar and turbulent flows agree well with the data from experiments and indicate that the boundary layer code is useful for these conditions. In the next two sections, applications for other gas models are considered.

Air in Chemical Equilibrium

Calculated heat transfer rate distributions for laminar flow over a 45° spherically blunted cone with $r_N = 1.0$ ft are presented in figure 7 and compared with viscous shock layer (VSL) calculations obtained by Gupta, Lee, and Zoby using the method described in reference 25. The free-stream conditions correspond to a flight Mach number of 15 at an altitude of 80 000 ft. Three solutions with the present method are presented based on three different assumptions to obtain the edge conditions. The first case, labeled *blunt cone*, follows a classical boundary layer approach and uses properties along the surface streamline obtained from an inviscid, blunt-cone flow-field solution. Because the flow along an inviscid surface streamline has passed through a normal shock wave, the entropy along this streamline is constant and has a high value equal to that downstream of a normal shock. For this case the present results are slightly lower than the VSL results, with the difference increasing downstream.

The second case, labeled *sharp cone*, also follows a classical approach but uses an inviscid, sharp-cone flow-field solution. All inviscid flow for this case has passed through a relatively weak, constant-angle shock wave; thus, the entropy along the inviscid surface streamline is constant and has a relatively low value (much lower than for the blunt-cone case). Results for this case, shown only for $x/r_N \geq 2.0$, are higher than the VSL and blunt-cone results. This approach represents an upper limit for the laminar heating that will be reached far downstream of the stagnation point when all variable-entropy inviscid flow has been entrained in the boundary layer. This limit has obviously not been reached for these conditions.

The third case, labeled *variable entropy*, was computed by interpolation of the edge properties from the inviscid flow field at a distance equal to the boundary layer thickness away from the wall. The entropy at the edge of the boundary layer for this case is variable, starting at normal shock value at the stagnation point and decreasing downstream. The heating for this case is almost identical to the heating for the blunt-cone case for $0 \geq x/r_N \leq 2.0$ then departs and follows approximately the same level as did the VSL results. This progression clearly demonstrates the influence of variable-entropy edge conditions on the downstream heating. The stagnation-point heating is slightly lower (approximately 10 percent) than for the VSL. This difference may be attributed to differences in the thermodynamic or transport properties in the two codes.

Calculated surface heating rates from the present code are compared with experimental Reentry F flight data (ref. 26) in figure 8. The Reentry F configuration is a spherically blunted, 5° half-angle cone, 13 ft long, with an initial nose radius of 0.1 in. Inviscid edge conditions for these calculations were obtained from equilibrium-air, sharp-cone solutions (ref. 27). The comparisons presented in figure 8(a) are for 120 000 ft and a Mach number of 19.25. The flow for this case is laminar and the calculated heating agrees reasonably well with the experimental data.

Similar comparisons are presented in figure 8(b) for 80 000 ft, when the flow starts to become turbulent at a z/L location near 0.625. The calculations started with laminar flow at the nose and initiated "instantaneous" transition at $z/L = 0.625$. Both the laminar and the turbulent calculations agree well with the experimental data.

CF_4 Gas

Surface heat transfer distributions for flow over a sphere are presented in figure 9 along with experimental data measured in the Langley 20-Inch Mach 6 Tunnel (provided by Charles Miller of the Langley Space Systems Division). The CF_4 gas has a relatively low "effective γ" and is used to test blunt reentry configurations because it simulates the high-density ratio across the strong shock waves on these configurations in hypersonic flight. The flow is laminar and the predicted values agree well with the experimental data. This case illustrates the good application of the CF_4 chemistry package (from ref. 19) in the present code.

Concluding Remarks

An implicit finite-difference method has been used to obtain steady-flow solutions for axisymmetric, laminar, and turbulent boundary layer flow over several bodies and flow conditions. Results have been presented for laminar and turbulent flow of ideal gas, laminar flow of air in chemical equilibrium, and laminar flow in carbon tetrafluoride (CF_4). Most of the results were based on conditions of constant entropy at the boundary layer edge obtained from an inviscid flow-field solution at the surface.

Comparisons with experimental data have demonstrated that accurate solutions can be obtained with this approach. The method should prove useful as an analysis tool for comparisons with experimental wind tunnel data and for calculations of flight conditions wherein the assumptions of equilibrium air chemistry and constant entropy at the boundary layer edge are valid. In addition, the method can be extended to include variable boundary layer edge entropy effects.

NASA Langley Research Center
Hampton, VA 23681-0001
October 21, 1992

Appendix

Surface Heat Transfer Rate With Enthalpy Gradient

In general, for the laminar flow of a reacting gas with binary diffusion, the heat transfer to the surface can be written in the form

$$q_w = \left(k \frac{\partial T}{\partial y} + \rho \mathcal{D} \sum \mathrm{h}_i \frac{\partial \mathrm{c}_i}{\partial y} \right)_w \tag{A1}$$

where the first term on the right represents conduction and the second term represents diffusion. The symbol $\mathcal{D}$ is the binary diffusion coefficient, h_i is the enthalpy of the ith species, and c_i is the mass fraction of the ith species.

Now, for a reacting gas, the enthalpy is given by

$$\mathrm{h} = \sum \mathrm{c}_i \mathrm{h}_i \tag{A2}$$

Thus, $\partial \mathrm{h}/\partial y$ can be written as

$$\frac{\partial \mathrm{h}}{\partial y} = \sum \mathrm{c}_i \frac{\partial \mathrm{h}_i}{\partial y} + \sum \mathrm{h}_i \frac{\partial \mathrm{c}_i}{\partial y} \tag{A3}$$

Now,

$$\frac{\partial \mathrm{h}_i}{\partial y} = c_{p_i} \frac{\partial T}{\partial y} \tag{A4}$$

When this result is substituted into equation (A3), the following is obtained:

$$\frac{\partial \mathrm{h}}{\partial y} = \sum \mathrm{c}_i c_{p_i} \frac{\partial T}{\partial y} + \sum \mathrm{h}_i \frac{\partial \mathrm{c}_i}{\partial y} = c_p \frac{\partial T}{\partial y} + \sum \mathrm{h}_i \frac{\partial \mathrm{c}_i}{\partial y} \tag{A5}$$

Thus,

$$\frac{\partial T}{\partial y} = \frac{1}{c_p} \frac{\partial \mathrm{h}}{\partial y} - \frac{1}{c_p} \sum \mathrm{h}_i \frac{\partial \mathrm{c}_i}{\partial y} \tag{A6}$$

Substituting this result into equation (A1) obtains the following equation for the heat transfer:

$$q_w = \left(\frac{k}{c_p} \frac{\partial \mathrm{h}}{\partial y} - \frac{k}{c_p} \sum \mathrm{h}_i \frac{\partial \mathrm{c}_i}{\partial y} + \rho \mathcal{D} \sum \mathrm{h}_i \frac{\partial \mathrm{c}_i}{\partial y} \right)_w \tag{A7}$$

When the Lewis number N_{Le}, defined as

$$N_{Le} = \frac{\rho \mathcal{D} c_p}{k} \tag{A8}$$

is introduced, the surface heat transfer rate can be expressed as

$$q_w = \left\{ \frac{k}{c_p} \left[\frac{\partial \mathrm{h}}{\partial y} + (N_{Le} - 1) \sum \mathrm{h}_i \frac{\partial \mathrm{c}_i}{\partial y} \right] \right\}_w \tag{A9}$$

For $N_{Le} = 1$, the second term in equation (A9) is zero and the surface heat transfer rate becomes

$$q_w = \left(\frac{k}{c_p} \frac{\partial \mathrm{h}}{\partial y} \right)_w \tag{A10}$$

or

$$q_w = \left(\frac{\mu}{N_{Pr}} \frac{\partial \mathrm{h}}{\partial y} \right)_w \tag{A11}$$

where N_{Pr} is the Prandtl number. Similar results can be obtained for turbulent flow.

References

1. Flügge-Lotz, I.; and Blottner, F. G.: *Computation of the Compressible Laminar Boundary-Layer Flow Including Displacement-Thickness Interaction Using Finite-Difference Methods.* AFOSR 2206, U.S. Air Force, Jan. 1962.

2. Davis, R. T.; and Flügge-Lotz, I.: *Laminar Compressible Flow Past Axisymmetric Blunt Bodies (Results of a Second-Order Theory).* Tech. Rep. No. 143 (Grants AF-AFOSR-62-242 and AF-AFOSR-235-63), Div. of Engineering Mechanics, Stanford Univ., Dec. 1963.

3. Harris, Julius E.: *Numerical Solution of the Equations for Compressible Laminar, Transitional, and Turbulent Boundary Layers and Comparisons With Experimental Data.* NASA TR R-368, 1971.

4. Anderson, E. C.; and Lewis, C. H.: *Laminar or Turbulent Boundary-Layer Flows of Perfect Gases or Reacting Gas Mixtures in Chemical Equilibrium.* NASA CR-1893, 1971.

5. Blottner, F. G.: Chemical Nonequilibrium Boundary Layer. *AIAA J.*, vol. 2, no. 2, Feb. 1964, pp. 232 240.

6. Mayne, A. W., Jr.; and Adams, J. C., Jr.: *Streamline Swallowing by Laminar Boundary Layers in Hypersonic Flow.* AEDC-TR-71-32, U.S. Air Force, Mar. 1971. (Available from DTIC as AD 719 748.)

7. Anderson, E. Clay; Moss, James N.; and Sutton, Kenneth: Turbulent Viscous-Shock-Layer Solutions With Strong Vorticity Interaction. *J. Spacecr. & Rockets*, vol. 14, no. 1, Jan. 1977, pp. 32 37.

8. Hamilton, H. Harris; DeJarnette, Fred R.; and Weilmuenster, K. James: Application of Axisymmetric Analog for Calculating Heating in Three-Dimensional Flows. *J. Spacecr. & Rockets*, vol. 24, no. 4, July Aug. 1987, pp. 296 302.

9. Dorrance, William H.: *Viscous Hypersonic Flow.* McGraw-Hill Book Co., Inc., c.1962.

10. Hamilton, H. Harris, II; and Spall, John R.: *Time-Dependent Solution for Axisymmetric Flow Over a Blunt Body With Ideal Gas, CF_4, or Equilibrium Air Chemistry.* NASA TM-87675, 1986.

11. Blottner, F. G.: Finite Difference Methods of Solution of the Boundary-Layer Equations. *AIAA J.*, vol. 8, no. 2, Feb. 1970, pp. 193 205.

12. Davis, R. T.: Numerical Solution of the Hypersonic Viscous Shock-Layer Equations. *AIAA J.*, vol. 8, no. 5, May 1970, pp. 843 851.

13. Adams, John C., Jr.: *Implicit Finite-Difference Analysis of Compressible Laminar, Transitional, and Turbulent Boundary Layers Along the Windward Streamline of a Sharp Cone at Incidence.* AEDC-TR-71-235, U.S. Air Force, Dec. 1971.

14. Richtmyer, Robert D.; and Morton, K. W.: *Difference Methods for Initial-Value Problems,* Second ed. Interscience Publ., c.1967.

15. Peng, T. C.; and Pindroh, A. L.: *An Improved Calculation of Gas Properties at High Temperatures: Air.* D2-11722, Aero-Space Div., Boeing Co., Feb. 1962.

16. Van Driest, E. R.: On Turbulent Flow Near a Wall. *J. Aeronaut. Sci.*, vol. 23, no. 11, Nov. 1956, pp. 1007 1011, 1036.

17. Patankar, S. V.; and Spalding, D. B.: *Heat and Mass Transfer in Boundary Layers.* C.R.C. Press, 1968.

18. Clauser, Francis H.: The Turbulent Boundary Layer. Volume IV of *Advances in Applied Mechanics,* H. L. Dryden and Theodore von Kármán, eds., Academic Press, Inc., 1956, pp. 1 51.

19. Sutton, Kenneth: *Relations for the Thermodynamic and Transport Properties in the Testing Environment of the Langley Hypersonic CF_4 Tunnel.* NASA TM-83220, 1981.

20. Hansen, C. Frederick: *Approximations for the Thermodynamic and Transport Properties of High-Temperature Air.* NASA TR R-50, 1959. (Supersedes NACA TN 4150.)

21. Jackson, M. D.; and Baker, D. L.: *Interim Report Passive Nosetip Technology* (PANT) *Program. Volume III. Surface Roughness Effects, Part I. Experimental Data.* SAMSO-TR-74-86, Vol. III, Pt. I, U.S. Air Force, Jan. 1974. (Available from DTIC as AD B001 120.)

22. Dhawan, S.; and Narasimha, R.: Some Properties of Boundary Layer Flow During the Transition From Laminar to Turbulent Motion. *J. Fluid Mech.*, vol. 3, pt. 4, Jan. 1958, pp. 418 436.

23. Weilmuenster, K. James; and Hamilton, H. Harris, II: Computed and Experimental Surface Pressure and Heating on 70-Deg Sphere Cones. *J. Spacecr. & Rockets*, vol. 24, no. 5, Sept. Oct. 1987, pp. 385 393.

24. Coles, Donald: *Measurements in the Boundary Layer on a Smooth Flat Plate in Supersonic Flow III. Measurements in a Flat-Plate Boundary Layer at the Jet Propulsion Laboratory.* Rep. No. 20-71 (Contract No. DA-04-495-Ord 18), Jet Propulsion Lab., California Inst. of Technology, June 1, 1953.

25. Gupta, Roop N.; Lee, Kam-Pui; and Zoby, Ernest V.: Enhancements to the Viscous-Shock-Layer Technique. AIAA-92-2897, July 1992.

26. Zoby, Ernest V.; and Rumsey, Charles B.: *Analysis of Free-Flight Laminar, Transitional, and Turbulent Heat-Transfer Results at Free-Stream Mach Numbers Near 20 (Reentry F).* NASA TM X-2335, 1971.

27. Hamilton, H. Harris, II: Approximate Method of Predicting Heating on the Windward Side of Space Shuttle Orbiter and Comparisons With Flight Data. *Entry Vehicle Heating and Thermal Protection Systems: Space Shuttle, Solar Starprobe, Jupiter Galileo Probe,* Paul E. Bauer and Howard E. Collicott, eds., American Inst. of Aeronautics and Astronautics, Inc., c.1983, pp. 21 53.

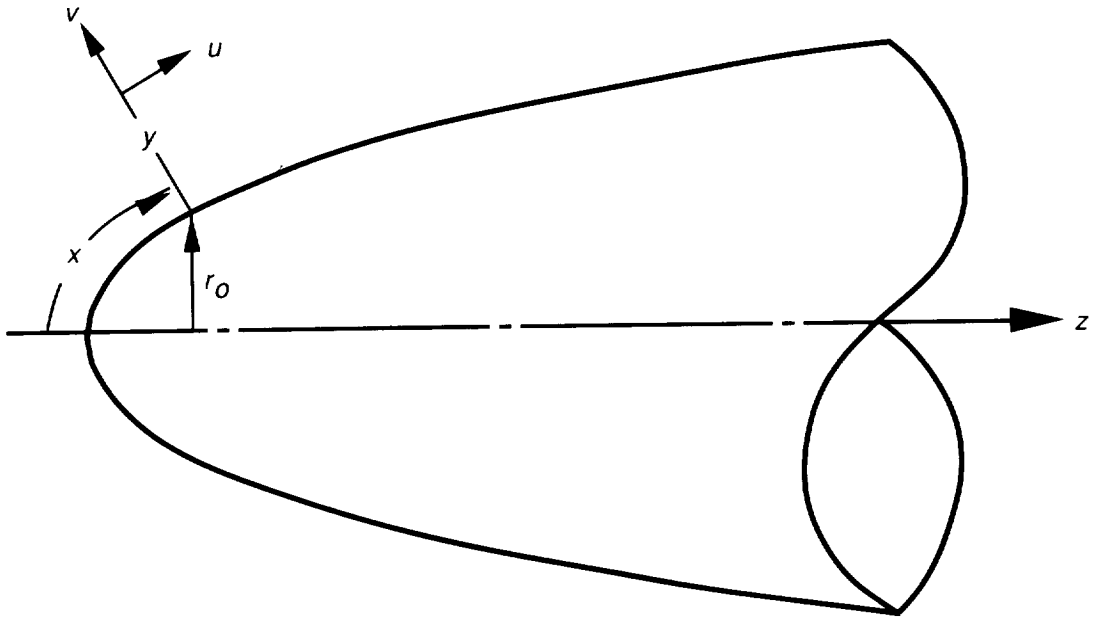

Figure 1. Definition of body-oriented coordinate system.

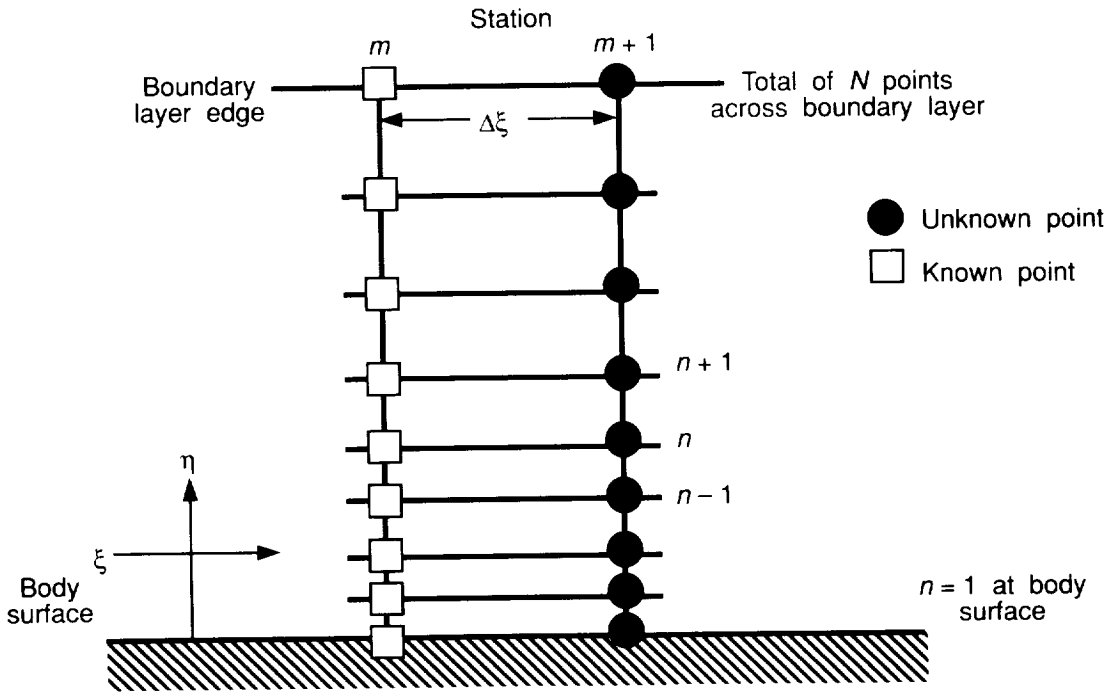

Figure 2. Typical grid system.

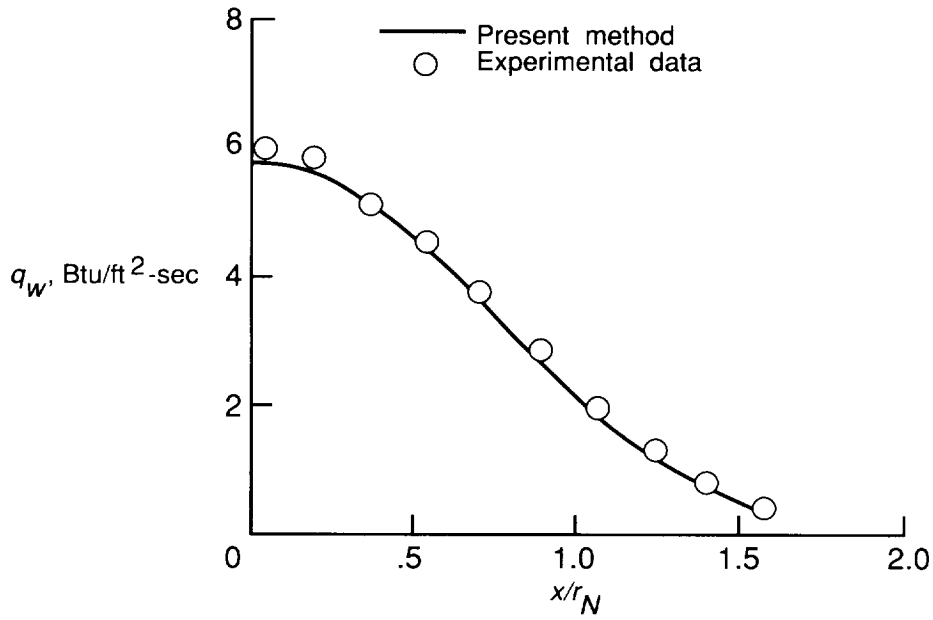

(a) $N_{Re} = 2.4 \times 10^5$ per foot; $M_\infty = 9.55$; $p_\infty = 0.6235$ lbf/ft^2; $T_\infty = 97.2°$R.

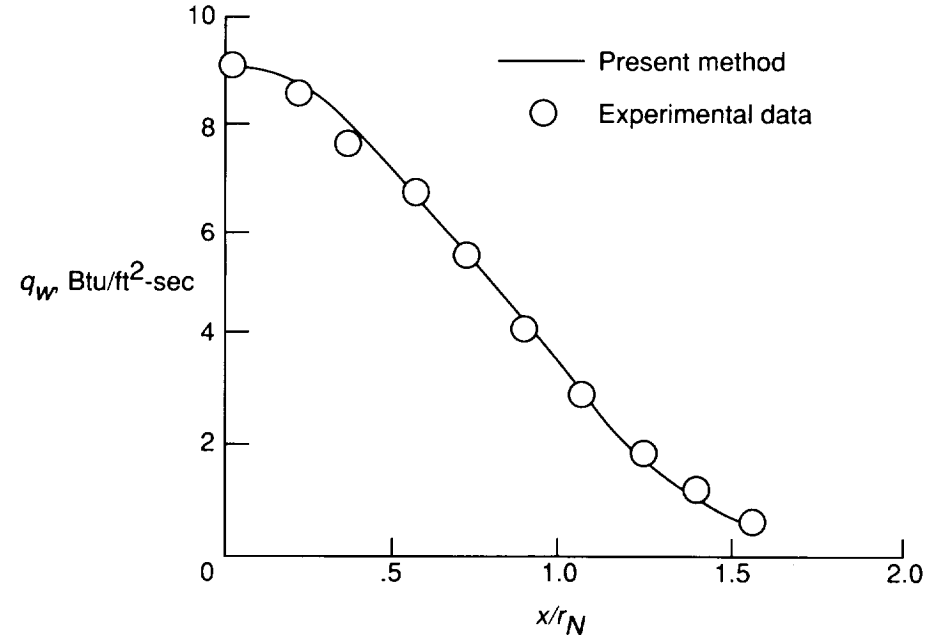

(b) $N_{Re} = 5.4 \times 10^5$ per foot; $M_\infty = 9.74$; $p_\infty = 1.362$ lbf/ft^2; $T_\infty = 95.7°$R.

Figure 3. Heat transfer rates on sphere in air. $\gamma = 1.4$; $r_N = 0.16667$ ft; $T_w = 540°$R.

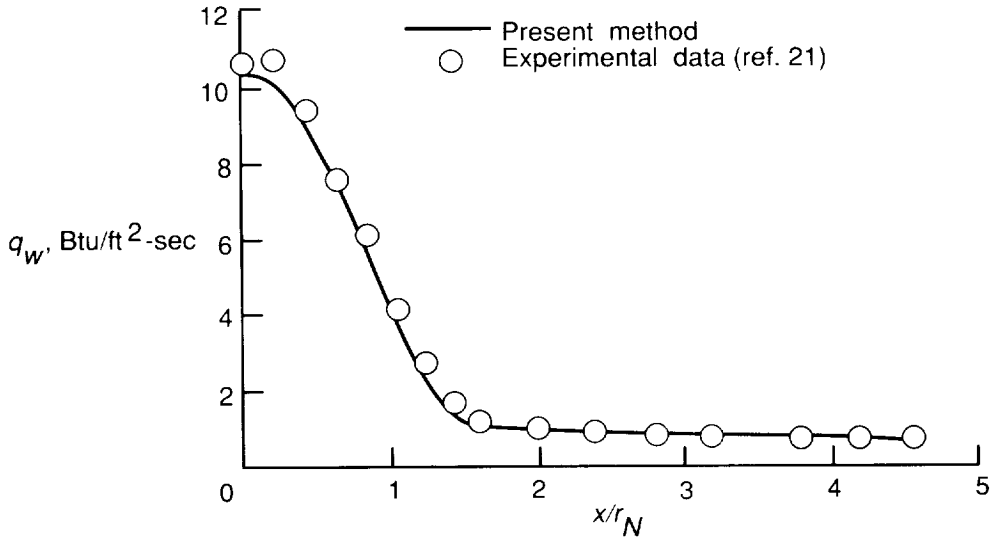

(a) $N_{Re} = 2.09 \times 10^6$ per foot. $p_\infty = 34.56$ lbf/ft^2; $T_\infty = 207.5°$R.

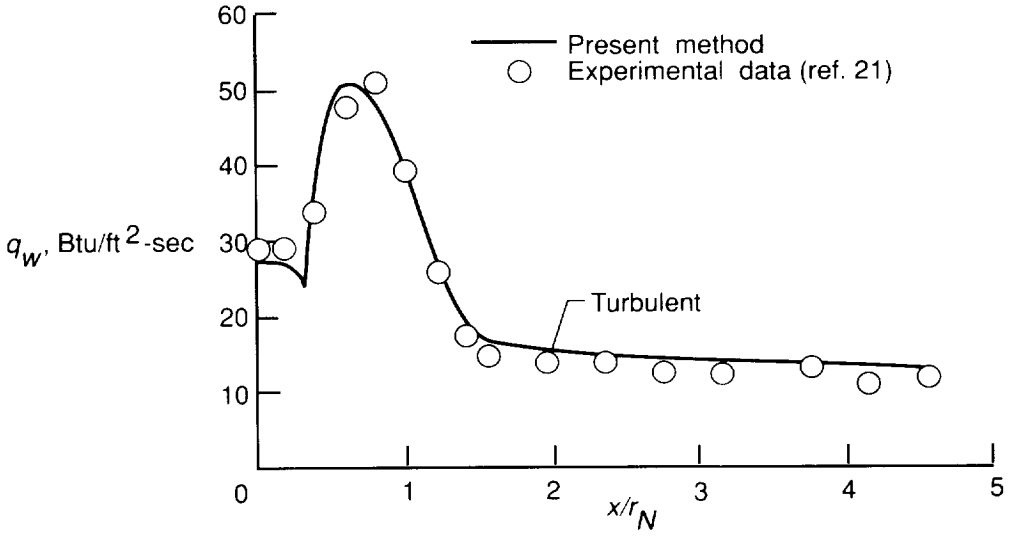

(b) $N_{Re} = 19.8 \times 10^6$ per foot. $p_\infty = 318.43$ lbf/ft^2; $T_\infty = 200°$R.

Figure 4. Heating on 8° sphere cone at $\alpha = 0°$. $M_\infty = 5$; $\gamma = 1.4$; $r_N = 0.2083$ ft.

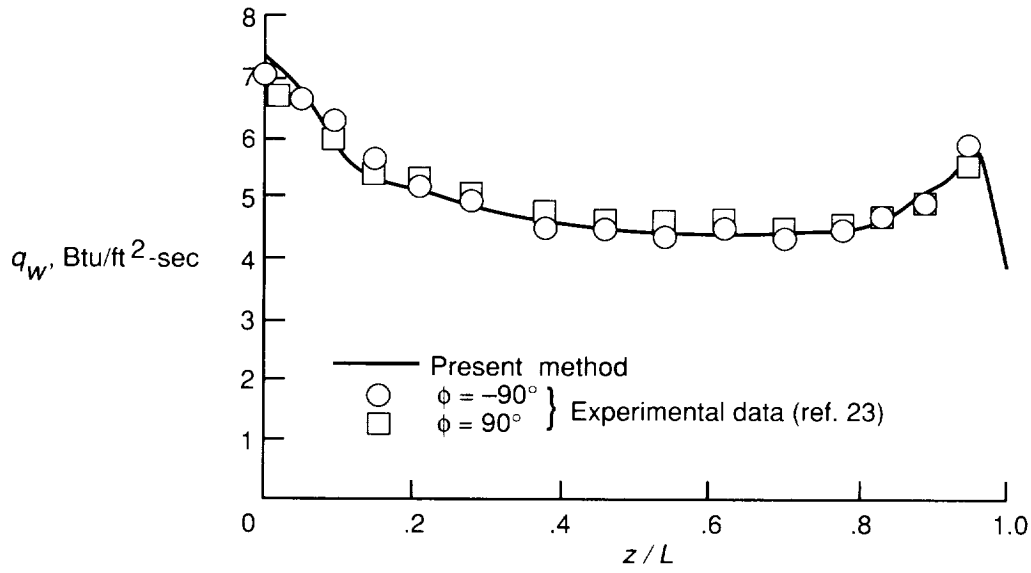

Figure 5. Heating-rate distribution on 70° half-angle sphere cone at $\alpha = 0°$. $M_\infty = 9.86$; $p_\infty = 1.28$ lbf/ft^2; $T_\infty = 84°$R; $r_N = 0.08333$ ft; $T_w = 550°$R.

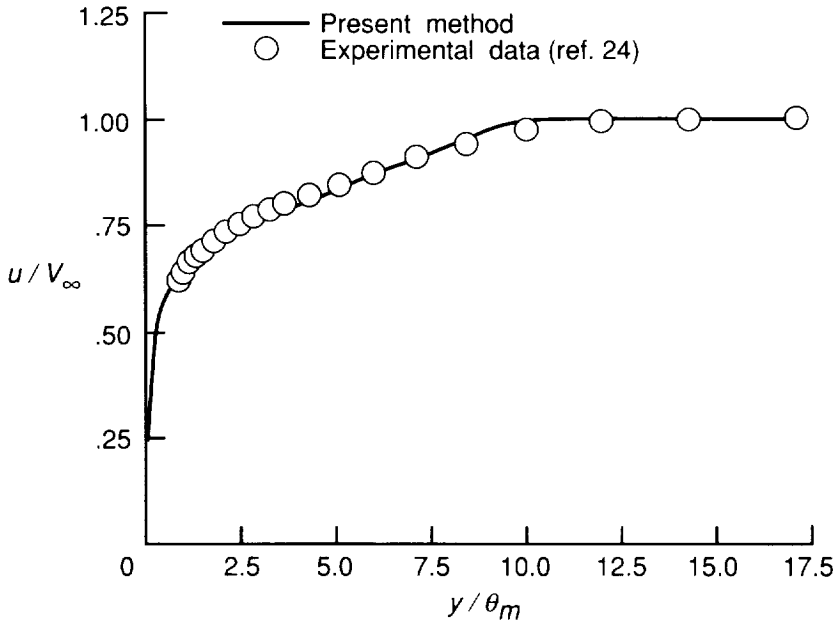

(a) $M_\infty = 1.982$. $p_\infty = 259.97$ lbf/ft^2; $T_\infty = 305.2°$R; $T_w = 452.0°$R.

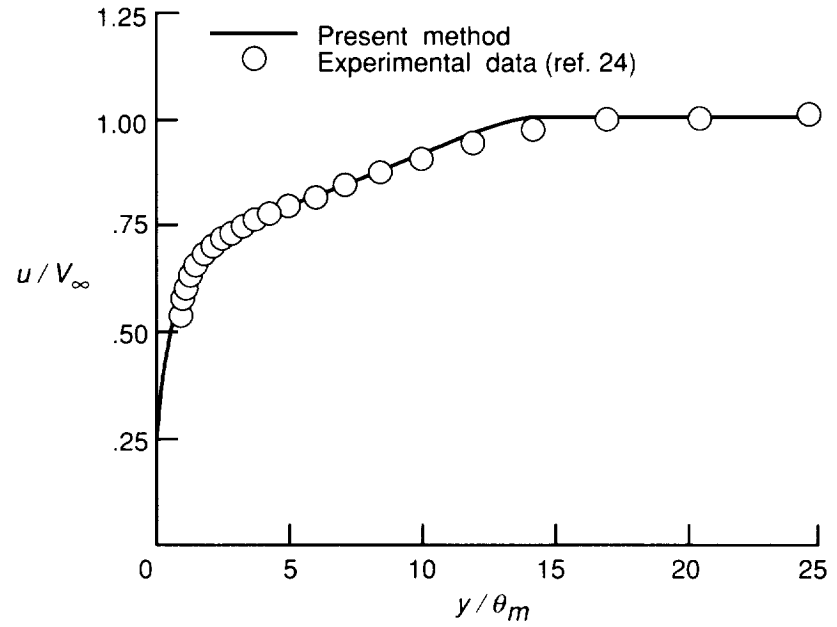

(b) $M_\infty = 3.701$. $p_\infty = 28.362$ lbf/ft^2; $T_\infty = 150.0°$R; $T_w = 401.2°$R.

Figure 6. Boundary layer on flat-plate velocity profile at $x = 1.79$ ft.

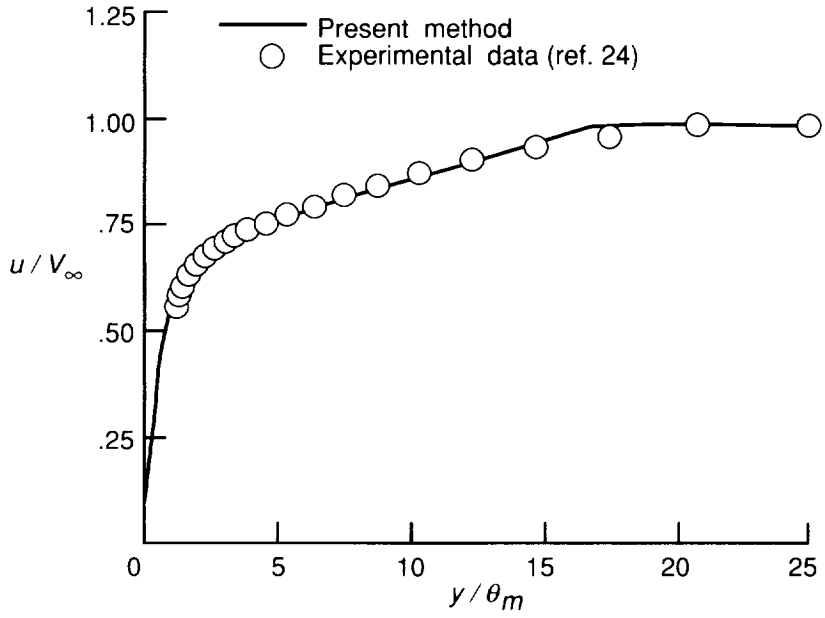

(c) $M_\infty = 4.554$. $p_\infty = 26.268$ lbf/ft^2; $T_\infty = 107.6°$R; $T_w = 374.7°$R.

Figure 6. Concluded.

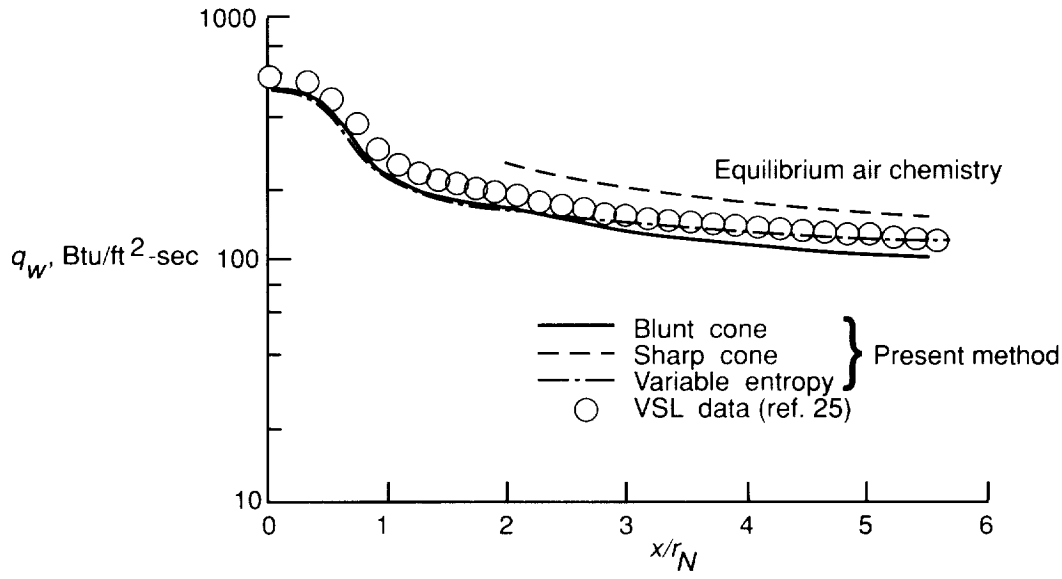

Figure 7. Heating-rate distribution on 45° half-angle sphere cone at $\alpha = 0°$. $M_\infty = 15$; $p_\infty = 58.5$ lbf/ft^2; $T_w = 398°$R; $r_N = 1.0$ ft; $T_{tr} = 1800°$R.

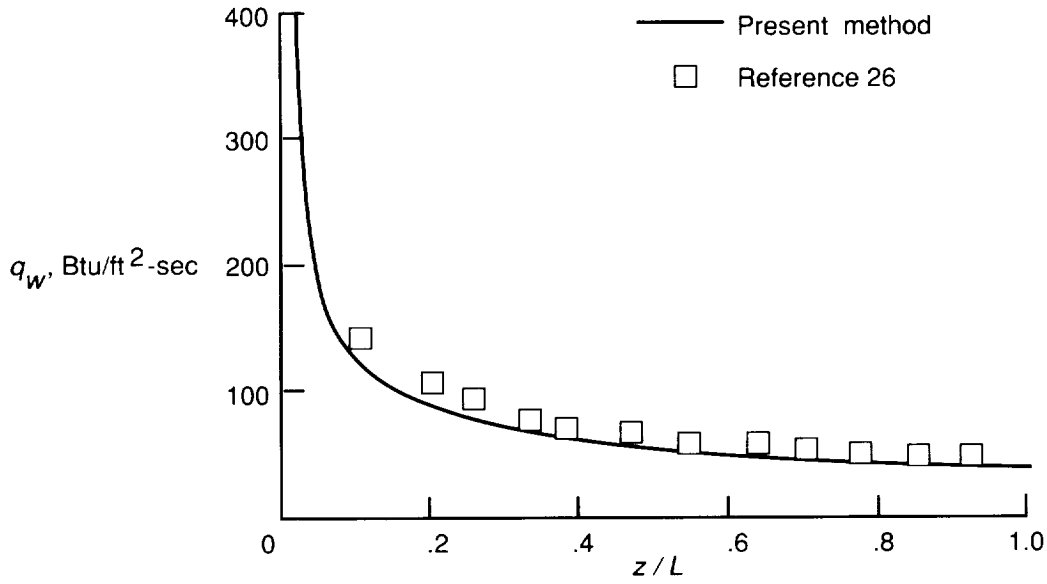

(a) Altitude = 120 000 ft. $M_\infty = 19.25$; $\alpha = 0°$.

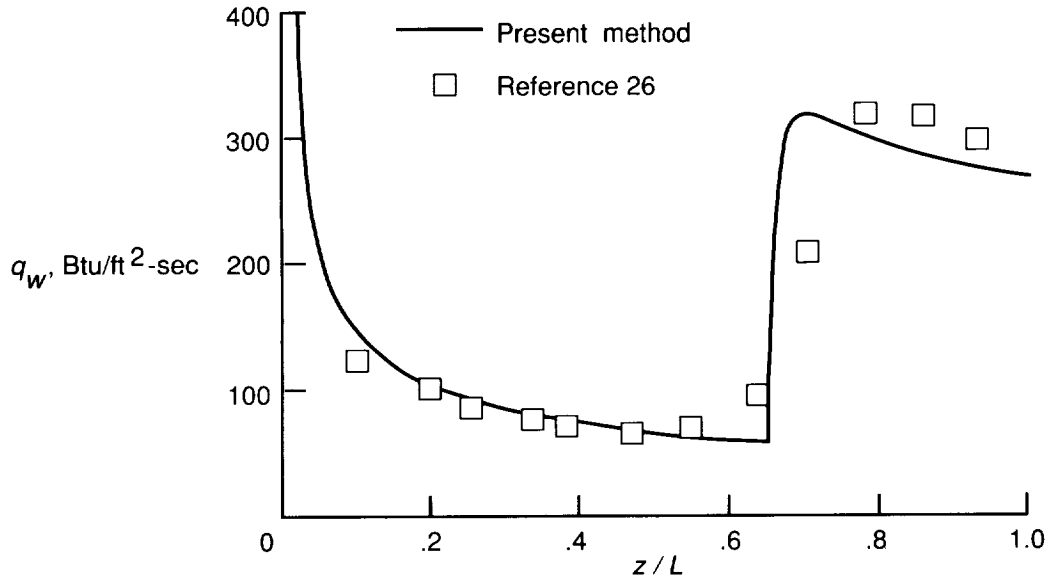

(b) Altitude = 80 000 ft. $M_\infty = 19.97$; $\alpha = -0.15°$.

Figure 8. Heating-rate distribution along cone for Reentry F.

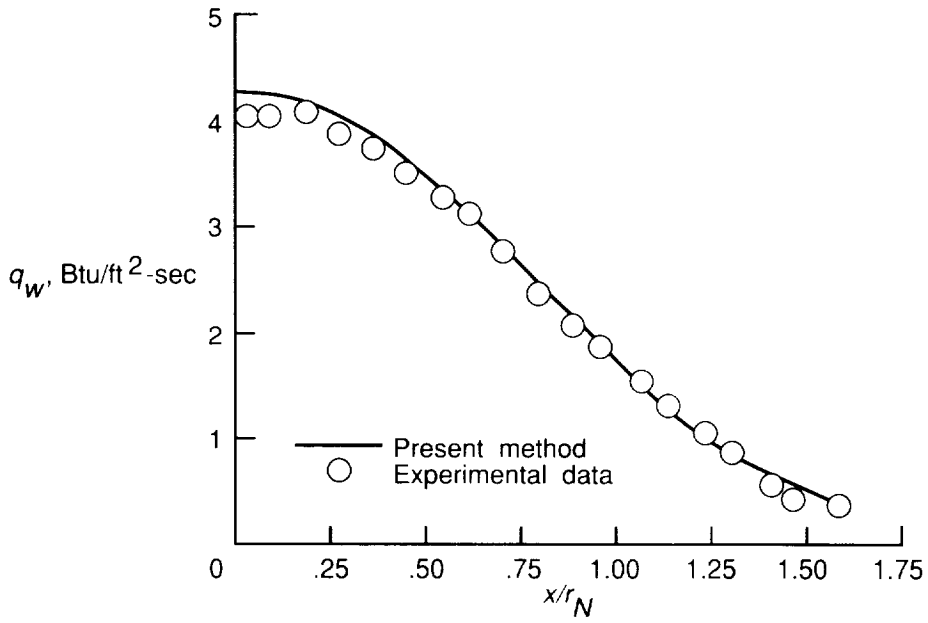

Figure 9. Heat transfer rate on sphere in CF_4. $M_\infty = 6.237$; $p_\infty = 3.9014$ lbf/ft^2; $T_\infty = 303.6°$R; $T_w = 579.6°$R; $r_N = 0.1667$ ft.

REPORT DOCUMENTATION PAGE

Form Approved
OMB No. 0704-0188

1. AGENCY USE ONLY *(Leave blank)*	2. REPORT DATE	3. REPORT TYPE AND DATES COVERED
	December 1992	Technical Paper

4. TITLE AND SUBTITLE
Finite-Difference Solution for Laminar or Turbulent Boundary Layer Flow Over Axisymmetric Bodies With Ideal Gas, CF_4, or Equilibrium Air Chemistry

5. FUNDING NUMBERS
WU 506-40-91-01

6. AUTHOR(S)
H. Harris Hamilton II, Daniel R. Millman, and Robert B. Greendyke

7. PERFORMING ORGANIZATION NAME(S) AND ADDRESS(ES)
NASA Langley Research Center
Hampton, VA 23681-0001

8. PERFORMING ORGANIZATION REPORT NUMBER
L-17102

9. SPONSORING/MONITORING AGENCY NAME(S) AND ADDRESS(ES)
National Aeronautics and Space Administration
Washington, DC 20546-0001

10. SPONSORING/MONITORING AGENCY REPORT NUMBER
NASA TP-3271

11. SUPPLEMENTARY NOTES
Hamilton: Langley Research Center, Hampton, VA; Millman: George Washington University, Joint Institute for Advancement of Flight Sciences, Hampton, VA; Greendyke: ViGYAN, Inc., Hampton, VA.

12a. DISTRIBUTION/AVAILABILITY STATEMENT
Unclassified Unlimited

Subject Category 34

12b. DISTRIBUTION CODE

13. ABSTRACT *(Maximum 200 words)*

A computer code has been developed that uses an implicit finite-difference technique to solve nonsimilar, axisymmetric boundary layer equations for both laminar and turbulent flow. The code can treat ideal gases, air in chemical equilibrium, and carbon tetrafluoride (CF_4), which is a useful test gas for hypersonic blunt-body simulations. This is the only known boundary layer code that can treat CF_4. Comparisons with experimental data have demonstrated that accurate solutions are obtained. The method should prove useful as an analysis tool for comparing calculations with wind tunnel experiments and for making calculations about flight vehicles where equilibrium air chemistry assumptions are valid.

14. SUBJECT TERMS	15. NUMBER OF PAGES
Boundary layer; Finite difference; Heat transfer	21
	16. PRICE CODE: A03

17. SECURITY CLASSIFICATION OF REPORT	18. SECURITY CLASSIFICATION OF THIS PAGE	19. SECURITY CLASSIFICATION OF ABSTRACT	20. LIMITATION OF ABSTRACT
Unclassified	Unclassified		

NSN 7540-01-280-5500

Standard Form 298(Rev. 2-89)
Prescribed by ANSI Std. Z39-18
298-102

NASA-Langley, 1992